

Layer-dependent exciton dynamics in InSe/WS_2 heterostructures

Siyao Li(李思垚), Yufan Wang(王雨凡), Zhiqiang Ming(明志强), Yong Liu(刘勇), Lanyu Huang(黄岚雨), Siman Liu(刘思嫚), Jialong Li(李佳龙), Yulin Chen(成昱霖), Zhoujuan Xu(徐周娟), Zeyu Liu(刘泽宇), Danliang Zhang(张丹亮), and Xiao Wang(王笑)

Citatio: Chin. Phys. B, 2025, 34 (**9**): 097802. DOI: 10.1088/1674-1056/adc6f7
http://cpb.iphy.ac.cn; http://iopscience.iop.org/cpb

What follows is a list of articles you may be interested in

Temperature-dependent photoluminescence of lead-free cesium tin halide perovskite microplates

Jiayu Tan(谭佳雨), Yixuan Zhou(周译玄), De Lu(卢德), Xukun Feng(冯旭坤), Yuqi Liu(刘玉琪), Mengen Zhang(张蒙恩), Fangzhengyi Lu(卢方正一), Yuanyuan Huang(黄媛媛), and Xinlong Xu(徐新龙)

Chin. Phys. B, 2023, 32 (**11**): 117802. DOI: 10.1088/1674-1056/ad028e

Anomalous photoluminescence enhancement and resonance charge transfer in type-II 2D lateral heterostructures

Chun-Yan Zhao(赵春艳), Sha-Sha Li(李莎莎), and Yong Yan(闫勇)

Chin. Phys. B, 2023, 32 (**8**): 087801. DOI: 10.1088/1674-1056/acc1d1

Enhanced photoluminescence of monolayer MoS_2 on stepped gold structure

Yu-Chun Liu(刘玉春), Xin Tan(谭欣), Tian-Ci Shen(沈天赐), and Fu-Xing Gu(谷付星)

Chin. Phys. B, 2022, 31 (**8**): 087803. DOI: 10.1088/1674-1056/ac657b

Exciton luminescence and many-body effect of monolayer WS_2 at room temperature

Jian-Min Wu(吴建民), Li-Hui Li(黎立辉), Wei-Hao Zheng(郑玮豪), Bi-Yuan Zheng(郑弼元), Zhe-Yuan Xu(徐哲元), Xue-Hong Zhang(张学红), Chen-Guang Zhu(朱晨光), Kun Wu(吴琨), Chi Zhang(张弛), Ying Jiang(蒋英),Xiao-Li Zhu(朱小莉), and Xiu-Juan Zhuang(庄秀娟)

Chin. Phys. B, 2022, 31 (**5**): 057803. DOI: 10.1088/1674-1056/ac380c

Magnetic polaron-related optical properties in Ni(II)-doped CdS nanobelts: Implication for spin nanophotonic devices

Fu-Jian Ge(葛付建), Hui Peng(彭辉), Ye Tian(田野), Xiao-Yue Fan(范晓跃), Shuai Zhang(张帅), Xian-Xin Wu(吴宪欣), Xin-Feng Liu(刘新风), and Bing-Suo Zou(邹炳锁)

Chin. Phys. B, 2022, 31 (**1**): 017802. DOI: 10.1088/1674-1056/ac0782

SPECIAL TOPIC — Exciton physics: Fundamentals, materials and devices

Layer-dependent exciton dynamics in InSe/WS_2 heterostructures

Siyao Li(李思垚)[1], Yufan Wang(王雨凡), Zhiqiang Ming(明志强), Yong Liu(刘勇), Lanyu Huang(黄岚雨), Siman Liu(刘思嫚), Jialong Li(李佳龙), Yulin Chen(成昱霖), Zhoujuan Xu(徐周娟), Zeyu Liu(刘泽宇), Danliang Zhang(张丹亮), and Xiao Wang(王笑)[†]

Key Laboratory for Micro-Nano Physics and Technology of Hunan Province, School of Physics and Electronics, College of Materials Science and Engineering, Hunan University, Changsha 410082, *China*

(Received 12 February 2025; revised manuscript received 26 March 2025; accepted manuscript online 31 March 2025)

Understanding interlayer charge transfer is crucial for elucidating interface interactions in heterostructures. As the layer number can significantly influence the interface coupling and band alignment, the charge transfer behaviors can be largely regulated. Here, we constructed two-dimensional (2D) heterostructures consisting of monolayer WS_2 and few-layer InSe to investigate the impact of InSe thickness on exciton dynamics. We performed photoluminescence (PL) spectroscopy and lifetime measurements on pristine few-layer InSe and the heterostructures with different InSe thicknesses. For pristine InSe layers, we found a non-monotonic layer dependence on PL lifetime, which can be attributed to the interplay between the indirect-to-direct bandgap transition and surface recombination effects. For heterostructures, we demonstrated that the type I band alignment of the heterostructure facilitates electron and hole transfer from monolayer WS_2 to InSe. As the InSe layer number increases, the reduction in conduction band minimum (CBM) enhances the driving force for charge transfer, thereby improving the transfer efficiency. Furthermore, we fabricated and characterized a WS_2/InSe optoelectronic device. By analyzing bias voltage dependent PL spectra, we further demonstrated that the trions in WS_2 within the heterostructure are positively charged (X^+), and their emission intensity can be efficiently modulated by applying different biases. This study not only reveals the layer-dependent characteristics of band alignment and interlayer charge transfer in heterostructures but also provides valuable insights for the applications of 2D semiconductors in optoelectronic devices.

Keywords: exciton, layer dependence, charge transfer, band alignment

PACS: 78.67.–n, 71.35.–y, 71.35.Pq

DOI: 10.1088/1674-1056/adc6f7 **CSTR:** 32038.14.CPB.adc6f7

1. Introduction

From bulk to monolayer,[1] two-dimensional (2D) semiconductors exhibit distinct optical and electrical properties, including spin-valley coupling,[1–4] enhanced excitonic effects,[5–8] and quantum Hall effect,[9] primarily due to quantum confinement effects and reduced dielectric screening. The variation in layer number introduces an additional degree of freedom, which significantly influences excitonic dynamics.[10–15] For instance, layer-dependent bandgap variations directly affect radiative recombination efficiency,[16,17] while reduced exciton binding energy with increased layer number has been shown to diminish exciton stability.[7,18] In heterostructures, the variation in the number of layers can significantly influence the charge transfer process. For instance, in the Bi_2O_2Se/WS_2 heterostructure, the change in Bi_2O_2Se thickness induces switching between type I and type II band alignments.[19] Increased layers of MoS_2 can enhance the charge transfer rate in QD/MoS_2 heterostructures.[20]

Indium selenide (InSe), with its tunable bandgap ranging from 1.25 eV in bulk to 2.1 eV in monolayer (ML), has high carrier mobility[9,21,22] and distinctive optical and electronic properties,[23–26] serving as an ideal platform for investigating layer-dependent phenomena.[27] Among its various phases (β, ε-, and γ phases), ε-phase InSe exhibits considerable application potential and distinctive advantages due to its unique structural properties.[28,29] On the other hand, monolayer WS_2 is a typical transition metal dichalcogenide (TMD) material with a direct band gap and rich excitonic states.[30] Heterostructures combining InSe with varying layer thicknesses and monolayer WS_2 enable precise tuning of the conduction band offset (CBO), providing an ideal system for studying band alignment and interlayer charge dynamics. While the layer-dependent dynamics of thicker InSe (> 8 nm) have been investigated,[31] the properties of thinner few-layer (FL) InSe remain unexplored. Furthermore, the band alignment and microscopic mechanisms governing interlayer charge transfer between InSe with different thicknesses and ML WS_2 have not been revealed.

Herein, we systematically investigated the layer-dependent photoluminescence (PL) lifetime of InSe at room temperature, as well as the interfacial interactions between monolayer WS_2 and InSe under optical excitation. Our findings reveal that interfacial charge transfer in the heterostructure significantly modulates the optical properties of both constituent materials, and we further elucidated the underly-

[†]Corresponding author. E-mail: xiao_wang@hnu.edu.cn

© 2025 Chinese Physical Society and IOP Publishing Ltd. All rights, including for text and data mining, AI training, and similar technologies, are reserved.

ing mechanisms. Through the identification of type-I band alignment formation between ML WS_2 and FL InSe (> 3 layers),[32] we demonstrated that optically excited electrons and holes in WS_2 transfer to InSe. Additionally, we investigated the impact of InSe thickness variation on the excitonic states of WS_2 within the heterostructure, demonstrating the interplay between charge transfer and dielectric screening in governing exciton dynamics. Finally, through gate voltage modulation experiments, we conclusively identified the origin of trion formation, providing critical insights into the tunability of excitonic behavior within the heterostructure.

2. Experiment and method

2.1. Sample preparation

The ML WS_2 and FL InSe were prepared by mechanical exfoliation from high-quality bulk crystals (Nanjing MKNANO Tech. Co., Ltd. and HQ Graphene Inc.). The layer numbers of InSe and WS_2 were identified by analyzing PL spectra at room temperature. For optical and spectroscopic measurements, pristine InSe, WS_2, and their heterostructures were transferred onto SiO_2 or glass substrates using a dry transfer method under an optical microscope. For the WS_2/InSe device, electrodes were fabricated using standard electron-beam lithography (EBL, Raith 150 Two) and deposited onto the heterostructures through metal thermal evaporation.

2.2. Optical measurements

The PL lifetime measurements were performed using a 405 nm pulsed laser for excitation, with the signal collected by a time-dependent single-photon counting (TCSPC, PicoQuant HydraHarp 400) system. The fluorescence lifetime imaging microscopy (FLIM) was conducted using the TCSPC system combined with a PI scanning stage. The fluorescence emission from the heterostructure samples was collected by two single-photon avalanche diodes (APDs, PicoQuant PDM Series) via a 50/50 beam splitter. An 800 nm long-pass filter and a 700 nm short-pass filter were used to separate the emission signals of InSe and WS_2, respectively. The signals were collected using an oil-immersion objective lens (NA = 1.4). Samples for FLIM measurements were transferred onto glass substrates, while other measurements were performed on SiO_2 substrates. The steady-state PL spectra were excited by a 488 nm continuous-wave (CW) laser and recorded at room temperature with a liquid-nitrogen-cooled CCD (Symphony II) and spectrometer (Horiba iHR320).

3. Results and discussion

We prepared ε-InSe flakes from bulk crystals by mechanical exfoliation. To prevent the degradation of samples in air, the InSe flakes used in this study were encapsulated with polymethyl methacrylate (PMMA) and measured within 3 hours after exfoliation. Figures 1(a)–1(c) present bright-field optical image, PL intensity, and PL lifetime mapping of a typical few-layer InSe flake, respectively. The number of layers in this sample was determined as 4–6 layers (the areas of which are indicated by colored lines) based on the optical contrast and their PL spectra.[9,33] The InSe layers with different thicknesses all show uniform PL emission within the layer (Fig. 1(b)). The inset in Fig. 1(b) shows the line profile of PL intensity across different layers, the position of which is indicated by the white dashed line. As the number of layers increases from 4L to 6L, an increased PL intensity is clearly observed. For the PL lifetime image (Fig. 1(c)) taken by the fluorescence lifetime imaging microscopy (FLIM), the averaged PL lifetime dramatically decreases when the layer number increases from 4L to 6L.

We have further measured other InSe layers. Figure 1(d) shows the PL spectra of InSe layers ranging from 3L to 8L at room temperature. According to the photon energy of the emission peaks, we observed the decreased bandgap (from 1.73 eV to 1.25 eV) with increased layer number (from 3L to 8L), which is consistent with previous research.[9] Figure 1(e) presents the time-resolved photoluminescence (TRPL) of InSe with representative layer numbers (3L, 6L, 7L, and bulk of approximately 70 nm). Through single-exponential fitting of the experimental data, we fitted all the TRPL curves and obtained the PL lifetimes. Among these different layers, the bulk InSe shows the longest PL lifetime of about 5.95 ns. Surface recombination continues to dominate the carrier dynamics at this thickness. The prolonged PL lifetime originates from the reduced surface recombination effect. The PL lifetime of 7L (0.73 ns) is longer than that of 6L (0.55 ns), while the 3L shows a much longer lifetime of about 1.3 ns.

To give a comprehensive summary on the layer-dependent PL lifetime, we conducted systemic TRPL measurements on various InSe layers. After fitting the TRPL curves, the summarized PL lifetimes as a function of layer number are shown in Fig. 1(f), which exhibits a non-monotonic dependence on the layer number. With increased layer number, the PL lifetime decreases first and then increases, showing the observed shortest lifetime of about 0.6 ns at 6L. This non-monotonic dependence can be interpreted by the indirect-to- direct bandgap transition and the surface recombination. For few-layer InSe, the PL lifetime decreases as the number of layers increases from 3L to 6L, which is consistent with the layer number where the transition from indirect to direct bandgap occurs at about 6L.[29,34] For direct bandgap transition, the shorter PL lifetime is expected. Regarding thicker InSe, the surface recombination of photo-excited carriers dominates. The long lifetime observed in the thicker layer and bulk can be attributed to the reduced surface recombination.[31]

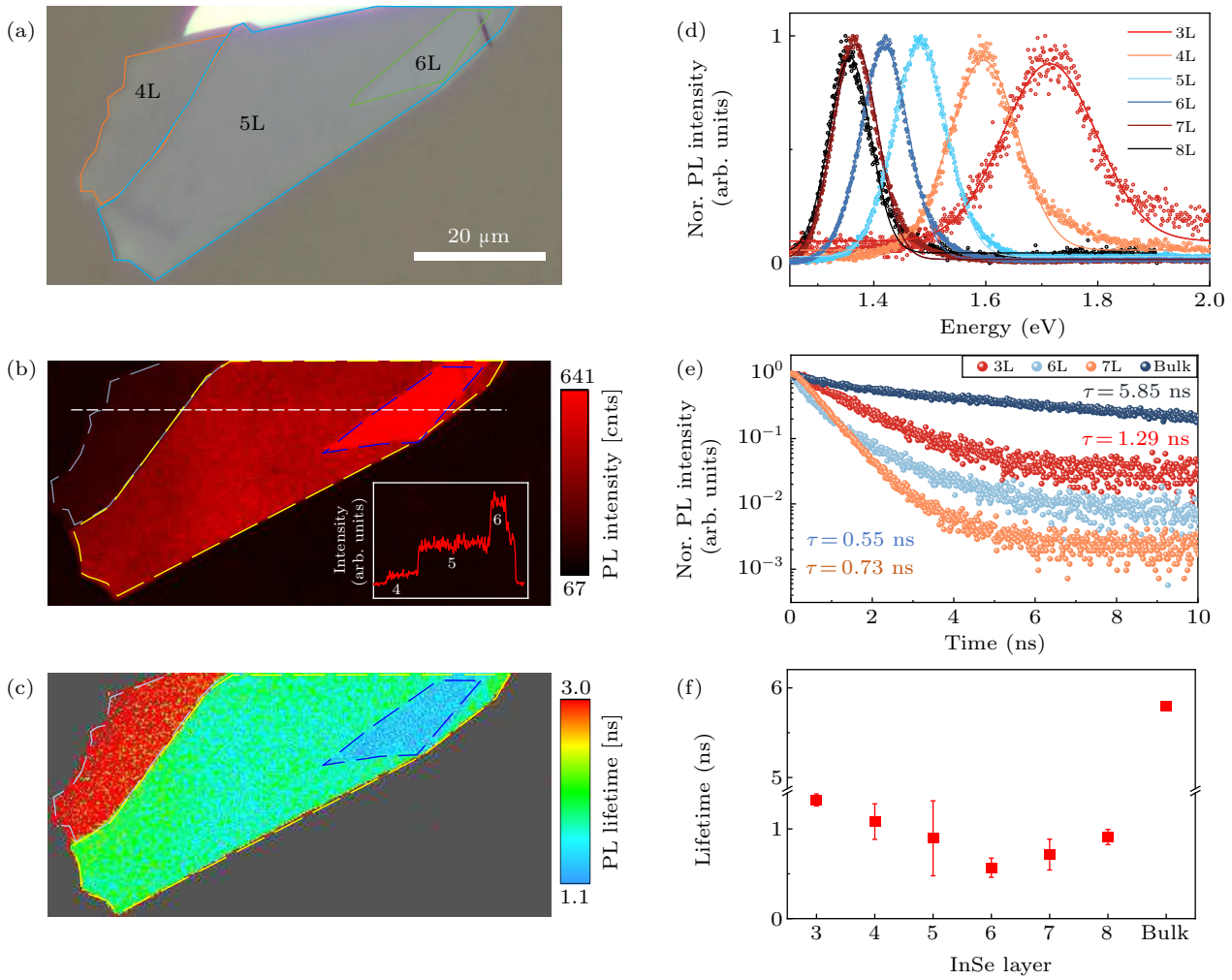


Fig. 1. (a) Optical image of InSe flakes with varying thicknesses, labeled as 4–6 layers (4L–6L). (b) and (c) PL intensity and lifetime mapping of the sample shown in (a). The inset shows the PL intensity profile along the white dashed line. (d) PL spectra of InSe layers ranging from 3 to 8 layers (3L–8L). (e) PL intensity decay curves of InSe with different layer thicknesses. (f) PL lifetime of InSe as a function of layer number.

We further investigated the optical properties of InSe/WS_2 heterostructures to explore the optical properties of FL InSe and its interaction with WS_2. Based on their band structures, FL InSe and monolayer WS_2 form the type-I band alignment in heterostructures, which leads to the transfer of photoinduced charge carriers from the wide-bandgap material (WS_2) to the narrow-bandgap material (InSe), as depicted in Fig. 2(a).[32] To confirm the band alignment, we performed KPFM measurements on a heterostructure consisting of monolayer WS_2 and 6L InSe. Figures 2(b) and 2(c) present the atomic force microscope (AFM) topography image and corresponding surface potential mapping of the heterostructure, respectively. The 6L InSe, WS_2, and heterostructure regions are determined by their heights. In Fig. 2(c), it is observed that the InSe has a higher surface potential than that of monolayer WS_2, indicating the electron transfer from WS_2 to InSe.

The band alignment at the interface of the heterostructure significantly impacts the optical properties of WS_2 and InSe compared to their pristine ones. Figure 2(d) presents the optical image of a heterostructure consisting of ML WS_2 and an InSe flake with different thicknesses. The InSe flake has thin layer areas covering from 4L to 8L and bulk areas. Figure 2(g) presents the PL intensity mapping of the sample with the WS_2 emission signal. Compared with the strong PL emission from pure monolayer WS_2, the heterostructure regions show clear PL intensity quenching due to charge transfer to InSe. In contrast, due to the charge transfer from monolayer WS_2, the PL intensity of InSe in the heterostructure enhances. As a representative case, Figs. 2(e) and 2(f) show the PL spectrum and TRPL of 6L-InSe in the heterostructure, as well as the corresponding data from pristine 6L-InSe for comparison. For 6L-InSe in the InSe/WS_2 heterostructure, the injection of electrons and holes from WS_2 via interfacial charge transfer leads to a twofold increase in PL intensity (Fig. 2(e)) and an extension of its PL lifetime (Fig. 2(f)), indicating reduced nonradiative recombination.

Figures 2(h) and 2(i) present the PL intensity and lifetime of InSe with different layer numbers in the heterostructure region (black solid circles) and pristine InSe (red open circles), respectively. As all black data points are above the red points, InSe in heterostructures exhibits enhanced PL intensity and enlarged PL lifetime due to electrons and holes from

WS_2. Notably, the increase in PL intensity observed in 6L is more pronounced than that in 4L, which is attributed to the larger conduction band offset. Since the CB offset between the two materials in the heterostructure is the critical factor influencing electron transfer, a larger offset enhances the driving force for charge transfer, thereby facilitating the charge transfer process.[20,35] For InSe layers thicker than 6L, the enhancement of PL intensity and extension of lifetime become less prominent, mainly due to the increased intrinsic carriers of InSe.

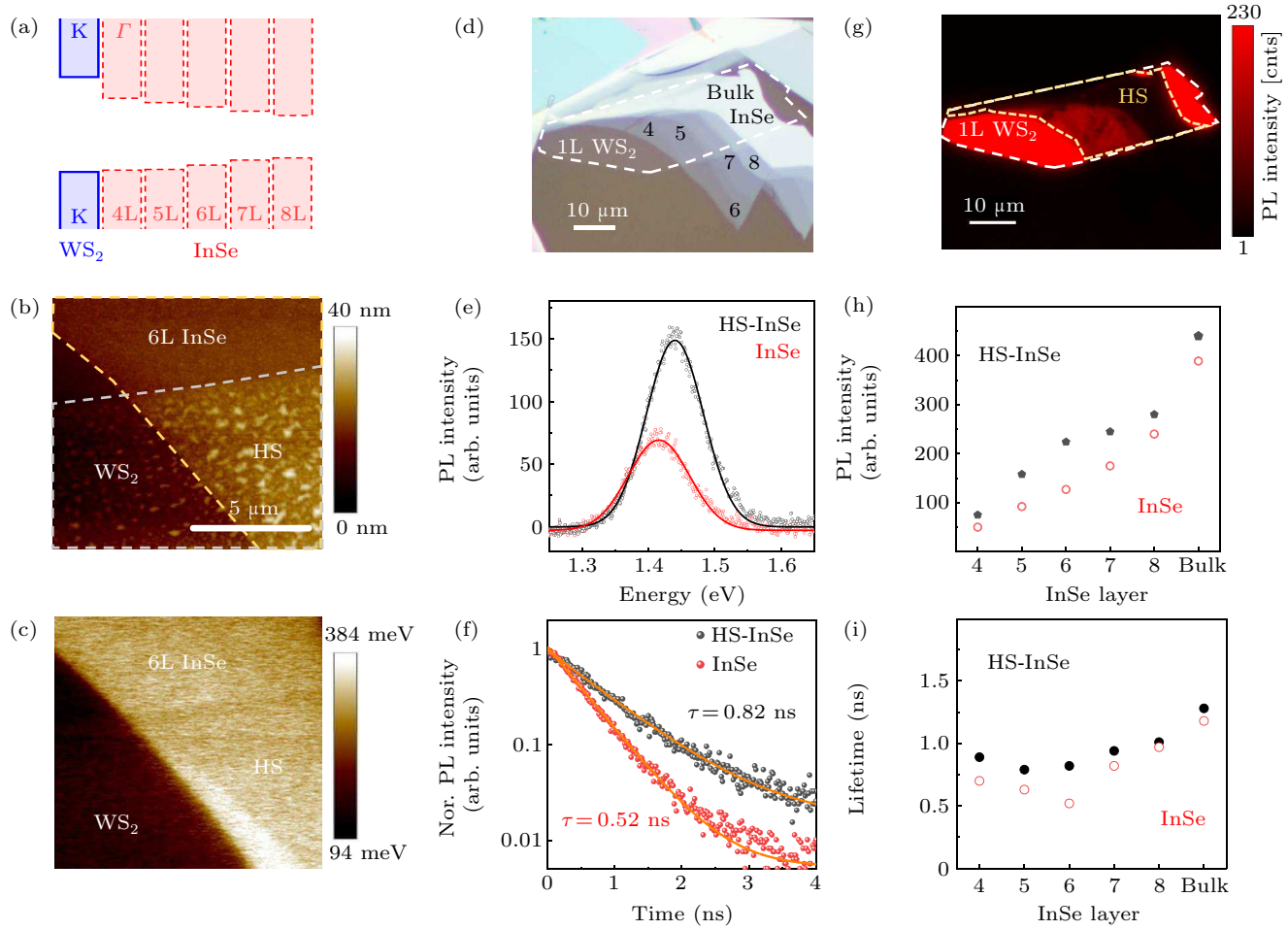


Fig. 2. (a) Band alignment of 48L-InSe/1L-WS_2. (b) AFM topography of 6L InSe and 1L WS_2. (c) Kelvin probe force microscopy (KPFM) of 6L InSe and 1L WS_2. (d) Optical images of InSe/WS_2 heterostructure. The white dashed lines indicate 1L WS_2. The layer number of InSe flakes is labeled. (e) and (f) show PL spectra and lifetime of 6L InSe in heterostructure and pristine InSe. (g) PL mapping of sample shown in (d). The pristine WS_2 and heterostructure regions are indicated by colored lines. (h) and (i) show PL intensity and lifetime of pristine InSe and InSe in heterostructures (HS-InSe) as a function of layer number.

To reveal the interfacial charge transfer effect on the emission properties of WS_2, we investigated the PL spectra and lifetime of WS_2 in InSe/WS_2 heterostructures with different InSe thicknesses (Fig. 3). Together with the data from pristine monolayer WS_2, we show the PL spectra of WS_2 in heterostructures with InSe layers varying from 4L to 8L and bulk InSe as well in Fig. 3(a). All spectra can be fitted with two peaks, which correspond to emissions from excitons located at 2.01 eV (red curves) and from trions located at 1.98 eV (green curves). The total PL intensities with different InSe layers are shown in the upper panel of Fig. 3(c), which exhibits a decreasing trend as the thickness of InSe increases. This observation agrees with the fact that the overall emission efficiency reduces due to the presence of trions. After fitting all spectra shown in Fig. 3(a), we obtained the ratio of trion to exciton PL emission intensity as a function of the InSe layer number (middle panel of Fig. 3(c)). Figure 3(b) presents the normalized TRPL of WS_2 in InSe/WS_2 heterostructures with different InSe thicknesses. By using double exponential fitting, we obtained the relationship between the PL lifetime of WS_2 and the InSe thickness, as shown in the bottom panel of Fig. 3(c).

As the number of InSe layers in the heterostructure increases, the ratio of trions and the lifetime of WS_2 show nonmonotonic dependence. These phenomena can be explained as follows. In InSe/WS_2 heterostructures, the CB offset is much larger than the VB offset, which leads to a significant transfer of electrons from WS_2 to InSe. This electron transfer causes the accumulation of holes in WS_2, thereby promoting the formation of trions. As the number of InSe layers increases

from 4L to 6L, the CB offset becomes larger, enhancing charge transfer efficiency and hence increasing the ratio of trions. When the InSe thickness exceeds 6L, the tunability of the InSe bandgap with layer thickness is reduced, and the CB offset increases only slightly. Meanwhile, the increase in dielectric constant begins to influence the exciton binding energy.[7,18] For heterostructures with thicker InSe, the monolayer WS_2 experiences the surrounding with a larger dielectric constant, which reduces the exciton binding energy in WS_2. Because trions are more sensitive to the dielectric environment,[36] the ratio of trions decreases in heterostructures with thicker InSe. Regarding the PL lifetime of WS_2, from 4L to 6L, the observed reduction in lifetime is attributed to charge transfer. On the other hand, the increase in the dielectric constant leads to stronger dielectric screening, which weakens the electron–hole interaction. This leads to a decrease in the overlap between the wavefunctions of electrons and holes, thereby reducing the radiative recombination rate and prolonging the PL lifetime.

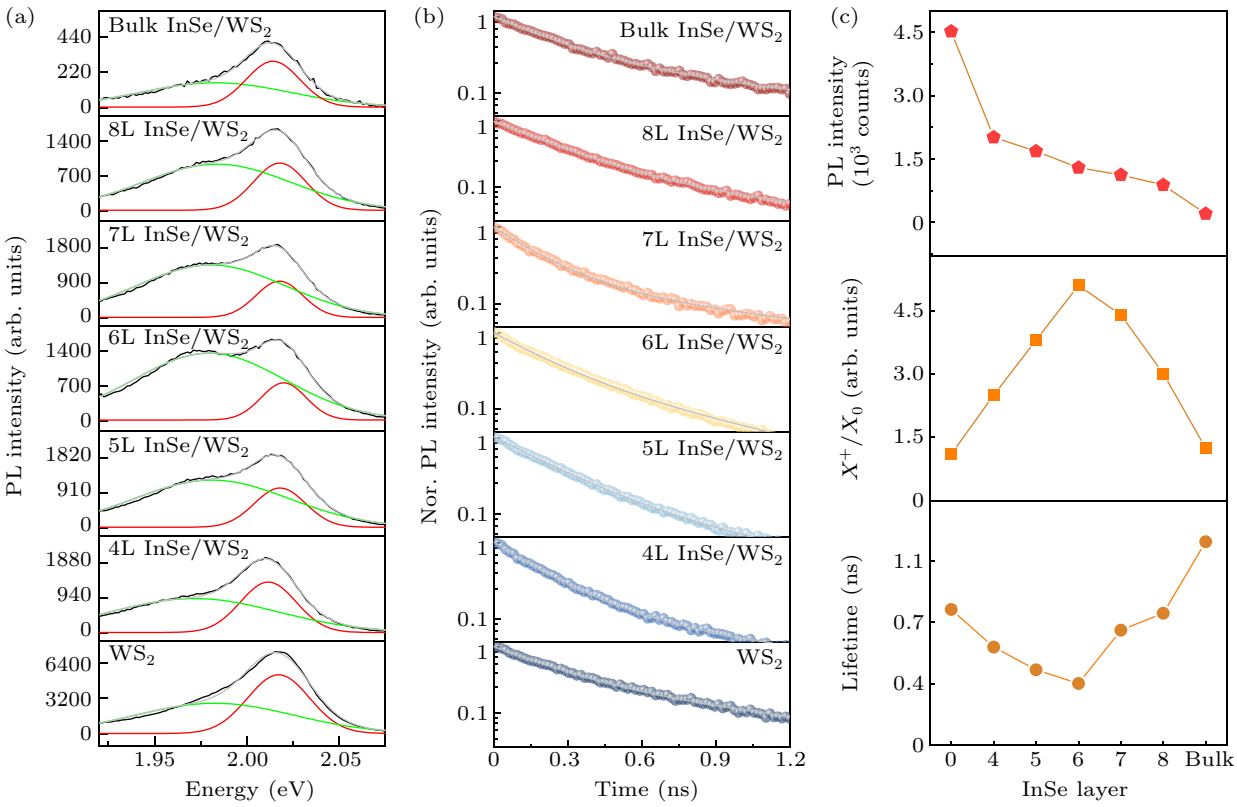


Fig. 3. (a) PL spectra of WS_2 in InSe/WS_2 heterostructures with different layer numbers. (b) PL decay curves of WS_2 in different InSe/WS_2 heterostructures. (c) PL intensity, trion-to-exciton emission ratio (X^+/X_0), and lifetime of WS_2 as a function of InSe layer number.

Therefore, we consider that the variations in the trion ratio and PL lifetime are governed by two competing factors: enhanced charge transfer efficiency and increased dielectric constant. On one hand, charge transfer reduces the PL lifetime and enhances hole accumulation, promoting the formation of trions; on the other hand, an increased dielectric constant with thick InSe reduces the overall exciton binding energy and the radiative recombination rate in WS_2. According to the experimental observations, we propose that for 4L–6L InSe/WS_2 heterostructures, charge transfer dominates, whereas the dielectric effect dominates for thicker InSe/WS_2 heterostructures.

To further tune the excitonic states of WS_2 within the heterostructure, we fabricated a single-gate device based on InSe/WS_2 and investigated gate-voltage-dependent optical emission spectra. Figure 4(a) shows the device configuration and the corresponding optical image, where the areas of InSe and WS_2 are indicated by colored lines. The thickness of the InSe layers in this heterostructure is about 10 nm. The gate voltage was applied via the Si/SiO_2 substrate. Figures 4(b) and 4(c) present the PL mapping of the sample (the area of which is indicated by red dashed lines in Fig. 4(a)) at a gate voltage of -15 V for photon energies of 2.005 ± 0.1 eV (neutral exciton) and 1.99 ± 0.15 eV (trion), respectively. The WS_2 region within the heterostructure (labeled as HS-WS_2) exhibits reduced neutral exciton emission (Fig. 4(b)) and enhanced trion emission (Fig. 4(c)) compared to pristine WS_2. Figure 4(d) presents the PL spectra taken from WS_2 in the heterostructure under gate voltages varying from -15 V to 15 V. As discussed in Fig. 3, due to interfacial charge transfer to InSe, the trions formed in WS_2 in the heterostructure are positively charged (labeled as X^+), which is distinct from the typically observed negatively charged trions in mechanically exfoliated WS_2.[37] Under positive gate voltage, the PL emis-

sion of WS_2 increases, which is attributed to the neutralization of positively charged trions by gate-induced electrons, promoting the conversion of trions into neutral excitons. Conversely, under negative gate voltages, the PL intensity is reduced, further confirming that the trions of WS_2 in the InSe/WS_2 heterostructure are positively charged. This phenomenon clearly demonstrates that gate voltage regulation can effectively alter exciton PL emissions. Figure 4(e) presents a 2D plot of the normalized PL spectra of WS_2 in the heterostructure. This plot provides clear experimental evidence that trions and neutral excitons dominate the PL emission under negative and positive gate voltages, respectively. To further quantify the relative changes between trions and neutral excitons, Fig. 4(f) shows the ratio of integrated PL emission contributions from trions to neutral excitons in the heterostructure region as a function of gate voltage. The insets show two typical spectra at 15 V and −15 V with their spectral fitting of trion (red curves) and exciton (green curves) contributions. The ratio increases from 0.32 to 3.8 when the gate voltage changes from 15 V to −15 V, clearly demonstrating the impact of gate voltage on the trion ratio.

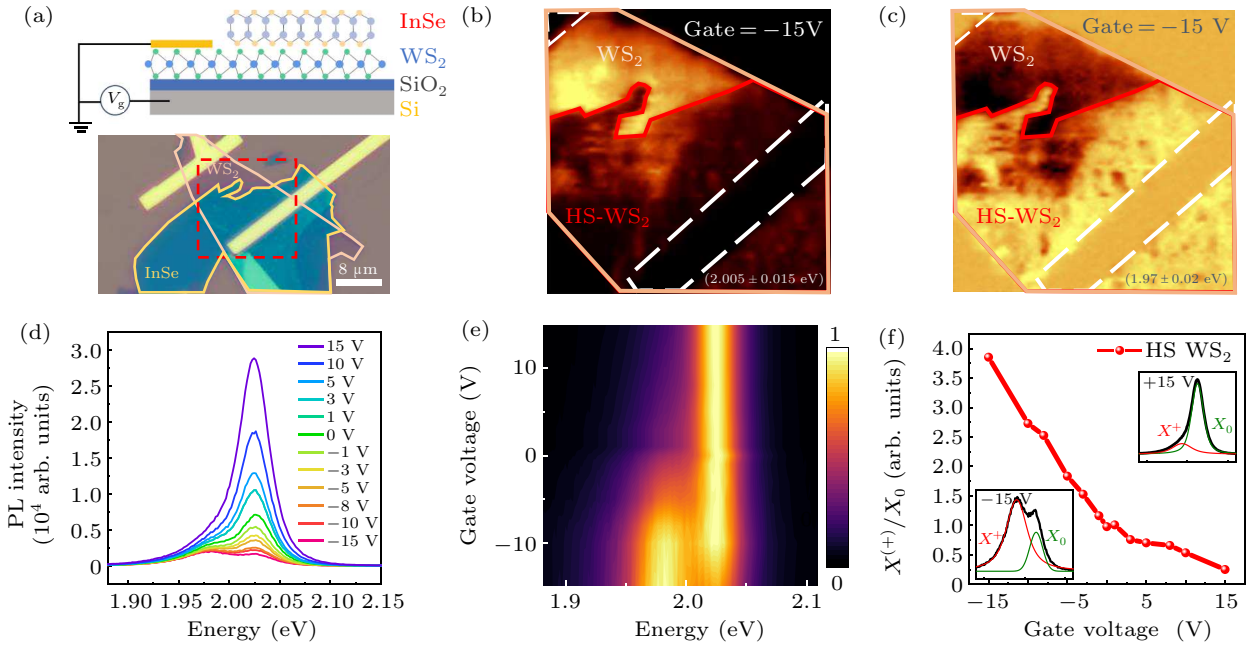


Fig. 4. (a) Device configuration and optical image of the InSe/WS_2 heterostructure. The scale bar is 10 μm. (b) and (c) PL mapping of the sample under a gate voltage of −15 V. The pristine WS_2 and heterostructure regions are indicated by colored lines. The white dashed lines indicate electrodes. (d) PL spectra of WS_2 in heterostructure under gate voltages varying from −15 V to 15 V. (e) 2D contour plot of normalized gate-dependent PL for WS_2 in heterostructure. (f) Integrated emission intensity ratio of X^+/X_0 of WS_2 in heterostructure under gate voltages ranging from −15 V to 15 V. The insets show the normalized PL spectra at −15 V and 15 V.

4. Conclusion and perspectives

In summary, we have carried out a systematic investigation of layer-dependent exciton dynamics in InSe/WS_2 heterostructures. Through layer-resolved PL lifetime measurements of FL InSe at room temperature, we demonstrated the crucial role of the indirect-to-direct bandgap transition. This transition enhances the radiative recombination efficiency of InSe by simultaneously increasing PL intensity and reducing PL lifetime, thereby providing deeper insights into its exciton dynamics.

By fabricating heterostructures comprising InSe layers of varying thickness and monolayer WS_2, we examined how charge transfer regulates the PL intensity and lifetime of InSe. Experimental results revealed that the type-I band alignment facilitates efficient charge transfer, enabling both electron and hole injection from WS_2 to InSe. This process enhances the PL intensity and extends the PL lifetime of InSe.

Through bandgap engineering, we further achieved precise modulation of the trion-to-exciton ratio in WS_2. Notably, our analysis identified 6L InSe as a critical thickness, where the conduction band offset is optimized to maximize charge transfer efficiency, resulting in the highest trion population and the shortest PL lifetime in WS_2. Beyond 6L, the enhanced dielectric screening effect weakens the influence of interlayer charge transfer on trion generation and PL lifetime, although charge transfer still suppresses the PL intensity of WS_2.

Moreover, gate voltage modulation experiments further elucidated the trion formation mechanism and highlighted the pivotal role of charge transfer in governing excitonic states. Considering carrier mobility, PL intensity, and the trion-to-exciton ratio, we conclude that the 6L InSe/ML WS_2 heterostructure offers the most promising potential for optoelectronic applications among the studied configurations.

Acknowledgments

This work was supported by the National Natural Science Foundation of China (Grant Nos. 92263107, U23A20570, 52221001, 62090035, and 52022029) and the Hunan Provincial Natural Science Foundation of China (Grant No. 2024RC1034).

References

[1] Ke C, Wu Y, Yang W, Wu Z, Zhang C, Li X and Kang J 2019 *Phys. Rev. B* **100** 195435
[2] Wang Y, Deng L, Wei Q, Wan Y, Liu Z, Lu X, Li Y, Bi L, Zhang L, Lu H, Chen H, Zhou P, Zhang L, Cheng Y, Zhao X, Ye Y, Huang W, Pennycook S J, Loh K P and Peng B 2020 *Nano Lett.* **20** 2129
[3] Xie W, Zhang L, Yue Y, Li M and Wang H 2024 *Phys. Rev. B* **109** 024406
[4] Ma H, Zhu Y, Liu Y, Bai R, Zhang X, Ren Y and Jiang C 2023 *Chin. Phys. B* **32** 107201
[5] Ye Z, Cao T, O'Brien K, Zhu H, Yin X, Wang Y, Louie S G and Zhang X 2014 *Nature* **513** 214
[6] Latini S, Olsen T and Thygesen K S 2015 *Phys. Rev. B* **92** 245123
[7] Lin Y, Ling X, Yu L, Huang S, Hsu A L, Lee Y H, Kong J, Dresselhaus M S and Palacios T 2014 *Nano Lett.* **14** 5569
[8] Ugeda M M, Bradley A J, Shi S F, da Jornada F H, Zhang Y, Qiu D Y, Ruan W, Mo S K, Hussain Z, Shen Z X, Wang F, Louie S G and Crommie M F 2014 *Nat. Mater.* **13** 1091
[9] Bandurin D A, Tyurnina A V, Yu G L, *et al.* 2017 *Nat. Nanotechnol.* **12** 223
[10] Liu Y, Hu X, Wang T and Liu D 2019 *ACS Nano* **13** 14416
[11] Wang T, Zhang Y, Liu Y, Li J, Liu D, Luo J and Ge K 2018 *J. Phys. Chem. C* **122** 18651
[12] Liu Y, Li H, Qiu C, Hu X and Liu D 2020 *Nano Res.* **13** 661
[13] Palummo M, Bernardi M and Grossman J C 2015 *Nano Lett.* **15** 2794
[14] Huo C F, Yun T, Yan X Q, Liu Z, Zhao X, Xu W, Cui Q, Liu Z B and Tian J G 2023 *Chin. Phys. B* **32** 067203
[15] Li J H, Bing D, Wu Z T, Wu G Q, Bai J, Du R X and Qi Z Q 2020 *Chin. Phys. B* **29** 017802
[16] Mudd G W, Svatek S A, Ren T, Patane A, Makarovsky O, Eaves L, Beton P H, Kovalyuk Z D, Lashkarev G V, Kudrynskyi Z R and Dmitriev A I 2013 *Adv. Mater.* **25** 5714
[17] Zhao W, Ghorannevis Z, Chu L, Toh M, Kloc C, Tan P H and Eda G 2013 *ACS Nano* **7** 791
[18] Weeraddana T M, Premathilaka S M, Tang Y, Antu A D, Roach A, Yang J and Sun L 2022 *J. Phys. Chem. Lett.* **13** 7756
[19] Zhang H, Fu J, Carvalho A, Poh E T, Chung J Y, Feng M, Chen Y, Wang B, Shang Q, Yang H, Zhang Z, Lim S X, Gao W, Gradečak S, Qiu C W, Lu J, He C, Sum T C and Sow C H 2024 *ACS Nano* **18** 16832
[20] Chen J S, Li M, Wu Q, Fron E, Tong X and Cotlet M 2019 *ACS Nano* **13** 8461
[21] Tsai T H, Yang F S, Ho P H, Liang Z Y, Lien C H, Ho C H, Lin Y F and Chiu P W 2019 *ACS Appl. Mater. Interfaces* **11** 35969
[22] Cao T, Hao S, Wu C, Pan C, Dai Y, Cheng B, Liang S J and Miao F 2024 *Chin. Phys. B* **33** 047302
[23] Brotons-Gisbert M, Proux R, Picard R, Andres-Penares D, Branny A, Molina-Sanchez A, Sanchez-Royo J F and Gerardot B D 2019 *Nat. Commun.* **10** 3913
[24] Tamalampudi S R, Lu Y Y, U R K, Sankar R, Liao C D, B K M, Cheng C H, Chou F C and Chen Y T 2014 *Nano Lett.* **14** 2800
[25] Liu Y, Zhong Q, Liang D, Jiang Q, Shuai Q, Yang X, Yi X, Sun X, Sun R, Zhong Y, Ge C, Tan Q, Luo Z, Chen S and Pan A 2023 *Laser Photonics Rev.* **17** 2300234
[26] Zhang B, Wu H, Peng K, Shen X, Gong X, Zheng S, Lu X, Wang G and Zhou X 2021 *Chin. Phys. B* **30** 078101
[27] Song C, Huang S, Wang C, Luo J and Yan H 2020 *J. Appl. Phys.* **128** 060901
[28] Hao Q, Yi H, Su H, Wei B, Wang Z, Lao Z, Chai Y, Wang Z, Jin C, Dai J and Zhang W 2019 *Nano Lett.* **19** 2634
[29] Wang Y, Zeng Z, Tian Z, Li C, Braun K, Huang L, Li Y, Luo X, Yi J, Wu G, Liu G, Li D, Zhou Y, Chen M, Wang X and Pan A 2024 *Adv. Mater.* **36** 2410696
[30] Wu J M, Li L H, Zheng W H, Zheng B Y, Xu Z Y, Zhang X H, Zhu C G, Wu K, Zhang C, Jiang Y, Zhu X L and Zhuang X J 2022 *Chin. Phys. B* **31** 057803
[31] Wu T H, Cheng H Y, Lai W C, Sankar R, Chang C S and Lin K H 2023 *Nanoscale* **15** 3169
[32] Ubrig N, Ponomarev E, Zultak J, *et al.* 2020 *Nat. Mater.* **19** 299
[33] Zheng T, Wu Z T, Nan H Y, Yu Y F, Zafar A, Yan Z Z, Lu J P and Ni Z H 2017 *RSC Adv.* **7** 54964
[34] Pike N A, Pachter R, Altvater M A, Stevens C E, Klein M, Hendrickson J R, Zhang H, Krylyuk S, Davydov A V and Glavin N R 2024 *J. Phys. Chem. C* **128** 7957
[35] Sun Z Y, Li Y, Xu B, Chen H, Wang P, Zhao S X, Yang L, Gao B, Dou X M, Sun B Q, Zhen L and Xu C Y 2021 *Adv. Opt. Mater.* **9** 2100438
[36] Kylänpää I and Komsa H P 2015 *Phys. Rev. B* **92** 205418
[37] Shang J, Shen X, Cong C, Peimyoo N, Cao B, Eginligil M and Yu T 2015 *ACS Nano* **9** 647